Eduvest – Journal of Universal Studies
Volume 5 Number 12, December, 2025
p- ISSN 2775-3735- e-ISSN 2775-3727

Innovative Investigation and Strategy for Improving the Performance of 70% Alumina Refractory Roofs Against Thermal-Slag Corrosion and Extreme Temperatures in Electric Arc Furnaces (EAF) in the Nickel Matte Production Process

Anggoro Rohadi, Sulistijono, Lukman Noerochim, Sutarsis, Hariyati Purwaningsih
Institut Teknologi Sepuluh Nopember, Indonesia
Email: anggoro.rohadi@gmail.com, ssulistijono@mat-eng.its.ac.id, lukman@mateng.its.ac.id, hariyati@mat-eng.its.ac.id, sutarsis@mat-eng.its.ac.id

ABSTRACT

This study investigates the performance of 70% alumina refractory on Electric Arc Furnace (EAF) roofs used in nickel matte smelting. Material characterization employed X-Ray Fluorescence (XRF), X-Ray Diffraction (XRD), and Scanning Electron Microscopy-Energy Dispersive X-ray (SEM-EDX). Thermodynamic simulations via FactSage and thermal stress analysis using Finite Element Analysis (FEA) complemented the study. Results show Al_2O_3 content drops below 16% in the corrosion zone while Fe_2O_3 increases, leading to corrosive phases like hercynite ($FeAl_2O_4$) and magnesium spinel ($MgAl_2O_4$). FactSage confirms stability of these phases at 1200–1400°C. FEA identifies maximum stress at the central roof zone, nearing the tensile strength limit of refractory materials. Mitigation strategies include optimizing brick geometry to reduce stress (short-term feasible), increasing alumina content while lowering Fe_2O_3 (effective but economically evaluated), and controlling furnace temperature distribution (most complex). These strategies bear practical significance for the nickel industry. Optimized brick design could extend Mean Time Between Relines (MTBR) from 12 to near 24 months, reducing refractory maintenance costs by 40–50%. This results in significant savings—approximately USD 1.3 million per intervention—in material and downtime costs. Enhanced refractory life also improves furnace stability and product quality. This study offers a comprehensive, innovative approach for designing more durable and reliable EAF refractories, supporting improved performance against thermal-slag corrosion and extreme temperatures in nickel matte production.

KEYWORDS *70% alumina, XRF, XRD, SEM-EDX, FactSage, FEA, EAF roofing*

INTRODUCTION

In the metal processing industry, especially nickel, the use of electric arc furnaces (EAF) is the main technology in the process of smelting nickel ore into nickel matte (Gupta & Kumar, 2020). This furnace operates with a large capacity to achieve the operational temperature required in the smelting process, which is around 1350°C to 1550°C (Zhao et al., 2019). The roof of the kiln is coated with 70% alumina-based refractory material, which is designed to withstand high temperatures and serves as thermal insulation during the melting process (Li & Wang, 2021). The refractory is intended to resist various types of attacks, whether thermal or chemical, during long operating cycles (Chen et al., 2020). However, in practice, degradation of refractory materials often occurs faster than expected (Rodrigues et al., 2022). This

degradation is caused by a combination of high-temperature exposure, slag corrosion, and repeated heating-cooling cycles (Hernández et al., 2020; Silva & Gomes, 2021).

Literature review (Darban et al., 2023; Andrés et al., 2020) affirms three main mechanisms: (1) corrosion of iron-magnesia oxide slag against the corundum matrix, (2) spinel formation that spurs volumetric expansion of 8–10%, and (3) repeated thermal spalling during daily tapping cycles (Kuang et al., 2025; Sun et al., 2025; Wang et al., 2020). However, most studies consider these mechanisms separately, focusing only on lab tests or simulations without integrating laboratory characterization and thermodynamic modeling (FactSage), as well as thermal stress analysis (FEA) based on actual industry data. Therefore, this study combines the perspective of on-site operations—which demand pragmatic and measurable solutions—with a systematic scientific approach to close the research gap and propose strategies to increase the life of the refractory (Abdelmoula et al., 2024; Zheng et al., 2022).

One of Indonesia's nickel processing facilities employs an integrated pyrometallurgical method, where laterite ore is mined and processed through stages of drying, calcination, smelting, and refining to produce nickel matte (Dalvi et al., 2020). A crucial stage involves smelting within an electric arc furnace, which operates at extreme temperatures between 1350°C and 1550°C to melt the calcine into matte and slag, a process powered by high-density energy from graphite electrodes (Zhang & Ostrovski, 2018). The furnace's refractory structure, particularly its roof made of 70% alumina material for thermal and chemical resistance, is critical yet vulnerable under these intense conditions (Li et al., 2021). Alumina refractories are widely used in pyrometallurgical furnaces due to their high-temperature strength and slag resistance (Chen et al., 2020). However, thermal shock, slag penetration, and mechanical stress often accelerate degradation in industrial operations (Rodrigues et al., 2022). These challenges highlight the importance of refractory performance optimization in sustaining furnace efficiency and operational safety (Silva & Gomes, 2021).

The primary operational challenge is the premature degradation of this refractory roof due to continuous exposure to high heat and chemical reactions with feed materials such as silica, iron, and magnesium. These interactions cause phenomena such as slagging and spalling, which drastically reduce the refractory's mechanical and thermal integrity. Consequently, the roof's thickness can degrade from an initial 9 inches to just 2 inches, with some sections collapsing entirely, as visually documented in incident reports. This failure sharply reduces the service life from a designed durability of two years to less than one year in practice.

This shortened lifecycle leads to significant repair cycles and financial impacts, dominating a considerable portion of the facility's operating costs. Historical data indicate that each furnace requires partial repairs annually and a complete relining every two years, with each major intervention costing millions of US dollars and halting production. The associated downtime results in production losses of approximately USD 1.3 million per event, underscoring a critical decrease in the Mean Time Between Relines (MTBR) from the target of 24 months to about 12 months. This situation highlights an urgent need for developing advanced material and technical solutions to extend refractory life and minimize operational disruptions.

RESEARCH METHOD

This study employed a multi-method approach to analyze the performance and degradation of alumina-based refractories in electric arc furnace roofs, integrating experimental laboratory tests, thermodynamic modeling, and thermal stress simulations. The research design proceeded through interconnected stages: first, experimental studies analyzed the chemical and

mechanical properties of refractory samples; second, thermodynamic modeling predicted chemical interactions between the refractory and slag; and third, finite element analysis simulated thermal and mechanical stress distributions. All stages were supported by technical data from manufacturers and field operations, with the collective aim of developing innovative strategies to enhance refractory durability and service life.

The experimental phase involved comprehensive material characterization. Sample preparation included cutting and labeling new and used refractory bricks from different furnace zones. Chemical analysis via X-ray fluorescence determined elemental composition, while X-ray diffraction identified and quantified crystalline phases. Furthermore, microstructure examination using scanning electron microscopy and energy dispersive X-ray spectroscopy revealed morphological details, porosity, and microcracks, providing a foundational understanding of the material's condition before and after use.

Thermodynamic modeling was conducted using FactSage software to simulate chemical equilibrium between the refractory and furnace feed at operational temperatures ranging from 800°C to 1400°C. Input data comprised the average chemical composition of the refractory and the calcine. The simulation setup utilized specific databases for oxide and slag systems, executing calculations to extract results such as the mass fraction of corrosive phases, the liquidus fraction, and the composition of solid phases. This analysis helped identify the formation of detrimental compounds like hercynite and spinels, which critically affected refractory integrity.

Finally, the insights from chemical modeling informed parameters for thermomechanical simulations performed in COMSOL Multiphysics. This finite element analysis modeled a refractory slab under steady-state thermal and mechanical loads, incorporating temperature-dependent material properties and boundary conditions replicating the furnace environment. The simulation mapped temperature distribution and calculated von Mises stress to identify failure-prone areas. Based on the consolidated findings from all methodologies, the study concluded by outlining a strategy for improvement, focusing on the development of new, more resistant refractory materials and the optimization of design and installation techniques to extend service life.

RESULTS AND DISCUSSION

This research aims to identify the properties and performance of new and used refractory, understand the degradation mechanism due to exposure to high temperatures and chemical reactions with process materials, and formulate improvement strategies based on scientific analysis and feasibility studies. The discussion was systematically arranged starting from the characterization of the new refractory as the initial condition, the characterization of the used refractory that has been degraded during the operation period whose sample point position is depicted in Figure 1, the evaluation of the chemical interaction between the process material and the refractory material, to the simulation of the thermal stress distribution and the proposed mitigation strategy. Each result was analyzed using a multiparameter approach that included visual testing techniques, X-Ray Fluorescence (XRF), X-Ray Diffraction (XRD), Scanning Electron Microscope – Energy Dispersive X-ray (SEM/EDX), as well as FactSage and Finite Element Analysis (FEA) software-based simulations.

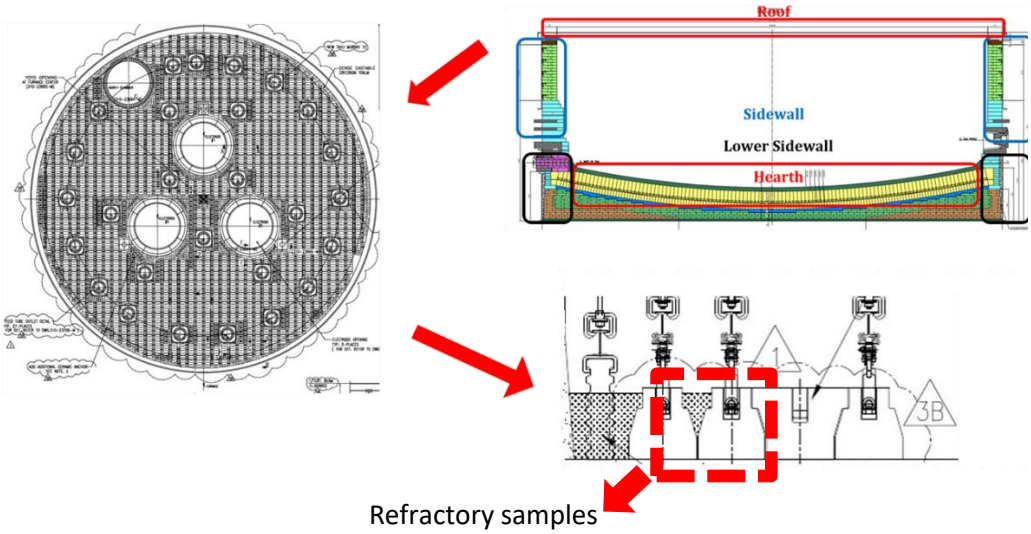

Figure 1. Refractory Sampling Position on Electric Furnace Roof (EAF)

By integrating the results of laboratory tests and numerical simulations, this chapter is expected to be able to comprehensively explain the mechanism of refractory performance reduction and provide technical justification for proposed technically and economically feasible improvement solutions.

New Refractory brick characterization

This subchapter discusses the characteristics of new refractory refractory used in electric furnaces. Testing was carried out by various material characterization methods such as visual observation, chemical analysis (XRF), crystalline phase identification (XRD), and observation of microstructure and elemental distribution (SEM/EDX). The data obtained provide an initial overview of the suitability of materials for high-temperature operating environments and potential resistance to chemical interactions from process materials.

Visual Observation

Visual observation samples are the initial stage to assess the physical condition of the refractory macroscopically. The new refractory samples tested were obtained from the furnace preparation area and have not been exposed to metallurgical operations. Based on observations, these refractories have a homogeneous, dense surface, and are free of large cracks or porosity that are visible to the naked eye. The dominant color on the brick surface is whitish beige, which shows the characteristics of high-temperature sintered alumina-silicate bricks. However, there is a slight brownish discoloration in some areas, especially on the underside of the brick surface. This discoloration is most likely caused by minor contamination or minor oxidation processes during storage or transportation before installation. These visual conditions indicate that new refractories are generally still in excellent condition and worthy of further study through advanced characterization methods.

Figure 2 presents a visual photograph of new and used refractory samples, while Figure 3 illustrates the test zones used in this study, which consist of cold face, transition zone, and

hot face. This division of zones is important to ensure an accurate representation of material characteristics in each part of the refractory structure.

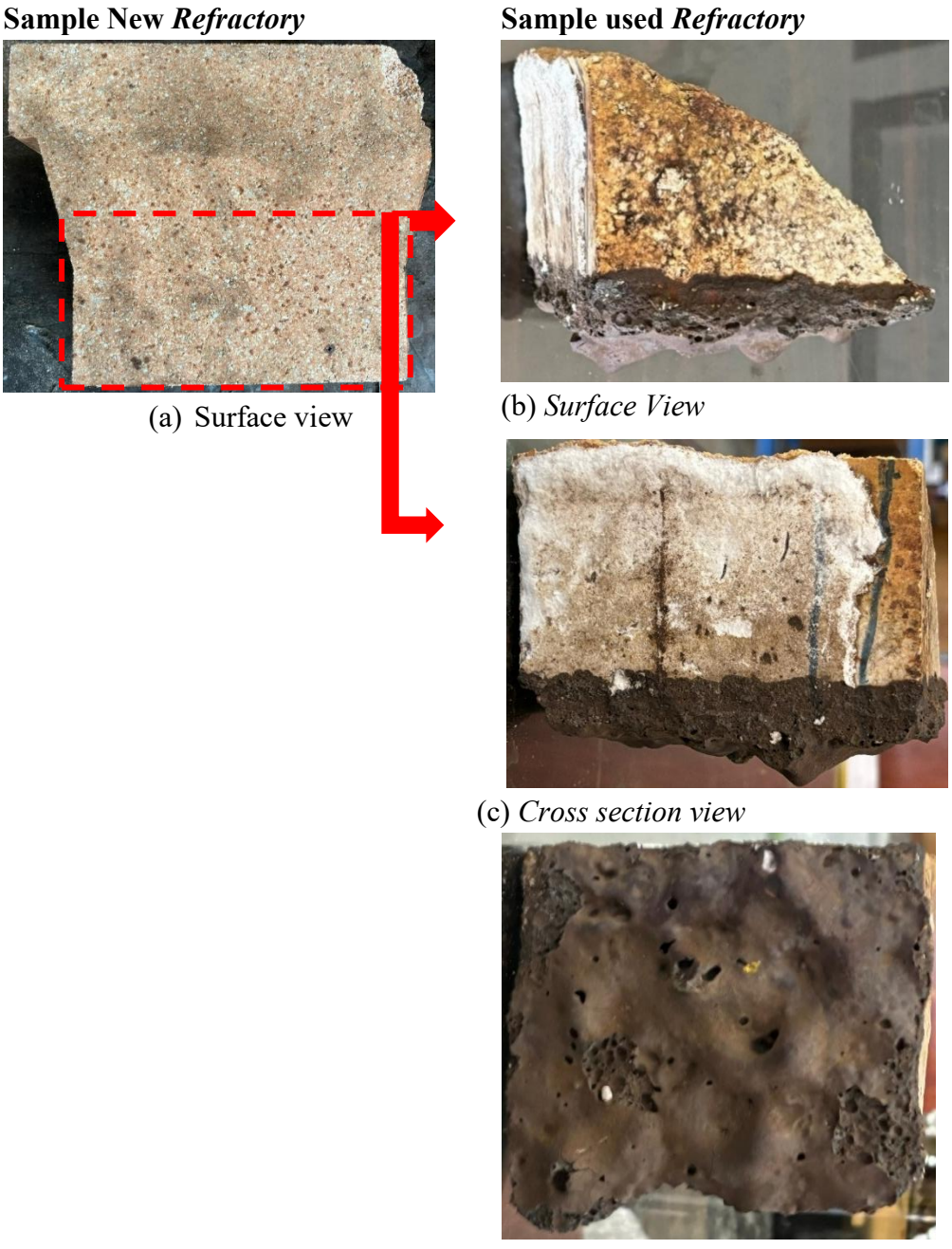

Figure 2. Visualization of Refractory Test Samples

The *new refractory* sample is a representation of the brick in its whole state as shown in Figure 2.a, while the red highlight box is an illustration of the brick part that is lost due to damage after use. Refractory brick undergoes a change where the bottom is covered with a blackish-brown layer as shown in Figure 2.b and Figure 2.c. Observations of the blackish-

brown layer showed that the part was uneven and porous (Figure 2.d), so further observation and analysis of refractory brick failures were needed.

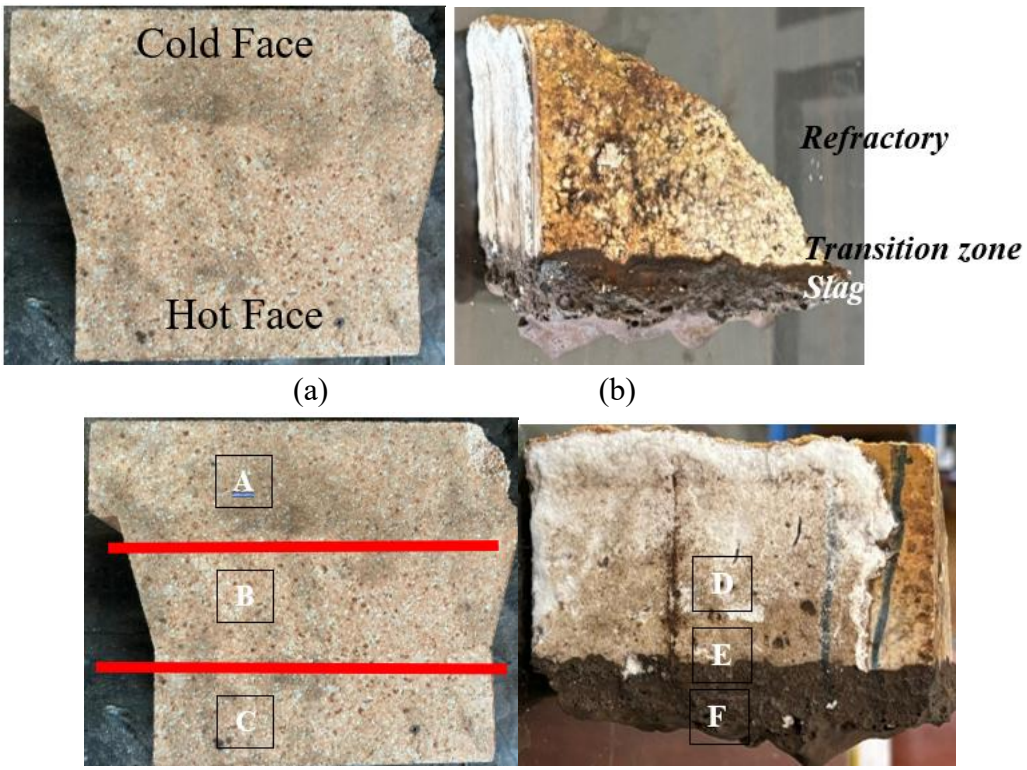

(a) (b)

(b) (d)

Figure 3. Visual Characterization and Zoning of New and Used Refractory Degradation

(a). New Refractory Sample – Transverse Appearance
(b). Used Refractory Samples – Identification of Degradation Zones
(c). Zoning A–C for New Refractory XRD Analysis
(d). D–F Zoning for Used Refractory XRD Analysis

Chemical Composition Analysis (XRF)

Chemical composition analysis using XRF aims to determine the content of the main oxide elements in the new refractories. The results of the analysis showed that the new refractory had an alumina (Al_2O_3) content of 39–45% and silica (SiO_2) of around 34–36%. In addition, there is a significant content of iron oxide (Fe_2O_3) of 11–12.5%, and phosphate (P_2O_5) of around 5.8–7.2%. The presence of other oxides such as MgO, CaO, Na_2O, and K_2O was also detected in minor amounts.

The comparison of the results of this test with the standard specifications of high alumina refractory (Table 1) shows a significant difference in composition, especially in alumina content lower than the standard of at least 70%. This condition indicates that this material may fall into the category of medium alumina bricks. Sufficiently high Fe_2O_3 and P_2O_5 content have the potential to reduce the corrosion resistance of materials, as both oxides can lower the local melting point and increase the rate of degradation at high temperatures. These findings are an early signal that requires further research to ensure the suitability of these materials in a highly aggressive furnace operating environment.

Table 1. XRF test results on New Refractory Samples

Chemical Composition	Result XRF (% Wt)	Standard(% Wt)
Al2O3	39,49 - 44,77	70,00 – 72,00
SiO2	34,00 – 36,00	22,00 – 24,00
CaO	1,30 – 1,40	2,80 – 3,00
TiO2	2,03 – 2,21	1,50 – 1,60
Fe2O3	11,00 – 12,5	0,20 – 0,30
P2O5	5,80 – 7,20	0,10 – 0,20
Na2O + K2O	1,10 – 1,20	0,30 – 0,50

Crystalline Phase Identification (XRD)

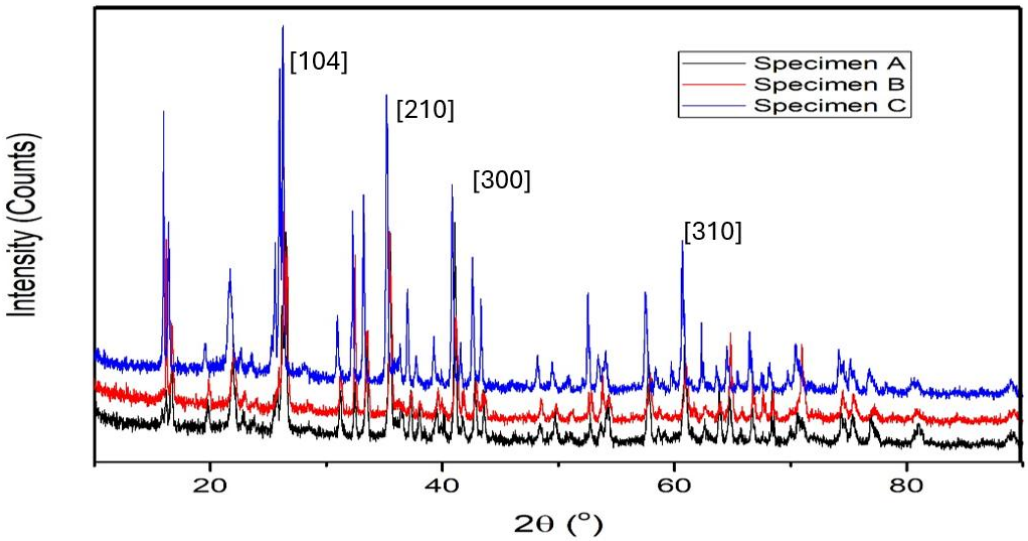

Figure 4. Plot of the diphragtogram of X-ray diffraction test results on a new refractory specimen,

Crystalline phase analysis using XRD provides information about the mineral structure present in the new refractory. The results of the XRD test showed the presence of main phases such as mullite (54.9%), sillimanite (30.4%), corundum (11.8%), and cristobalite (2.9%), as shown in Table 2.

Table 2. Qualitative and Quantitative Analysis of XRD Test Results on New Refractory Samples

Phase	Composition (%wt)
Aluminum Silicate - *Mullite* 3Al2O3.2SiO2	54,9
Aluminum Oxide - Corundum α-Al2O3	11,8
Silicon Oxide - Cristobalite SiO2	2,9
Aluminum Silicate - Sillimanite Al2SiO5	30,4

These phases are sintering products at high temperatures, and support the classification of materials as high alumina bricks from a mineralogy perspective. Theoretically, mullite contains 72% Al_2O_3, sillimanite 63% Al_2O_3, and corundum 100% Al_2O_3. If calculated based on the phase fraction and their respective composition:

Total estimated Al_2O_3:

$(0.549 \times 72\%) + (0.304 \times 63\%) + (0.118 \times 100\%) \approx 70.5\%$

XRD analysis confirmed that the Al_2O_3 content > 70% according to the specifications of high-alumina brick. XRF and XRD often provide different numbers due to the identification of material components from different angles: XRF measures the total oxide content (Al_2O_3, SiO_2, Fe_2O_3, etc.) in a sample, including all amorphous phases or binders. XRD only maps crystalline phases (e.g. corundum, mullite) through diffraction patterns. As a result, oxides that are in the form of glass or very fine particles do not give rise to XRD peaks but remain recorded in XRF, so the composition of total oxides (XRF) can be higher than the number of crystalline phases identified through XRD.

Microstructure and Element Mapping (SEM/EDX)

Observations of the microstructure and distribution of chemical elements were carried out to understand the environmental impact of electric furnace operation on the physical and chemical properties of refractory bricks. The Scanning Electron Microscopy (SEM) method is used to study changes in surface morphology and the relationships between grains at the microscopic level, while the Energy Dispersive X-ray Spectroscopy (EDX) technique is applied to map the spatial and semi-quantitative distribution of important elements. The combination of these two techniques is able to reveal indications of slag penetration, diffusion of foreign elements, and the formation of new phases as a result of chemical reactions and the influence of high temperatures during the furnace operating cycle. Analysis was performed on refractory samples before and after use, to compare the initial condition of the material with the actual damage in the field, so that degradation patterns that occurred both morphologically and compositionally could be identified.

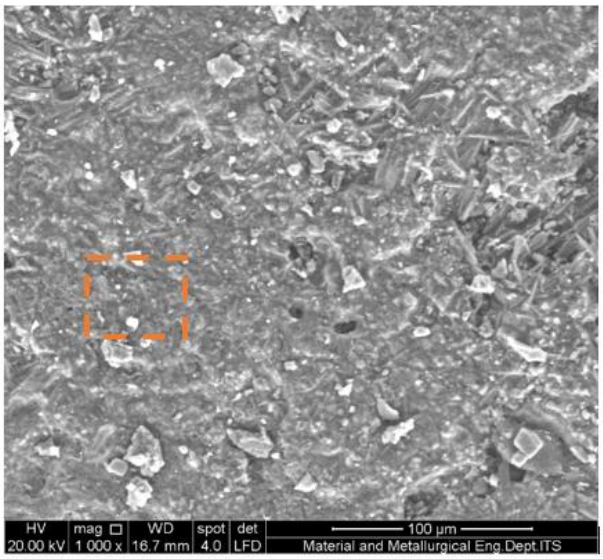

Figure 5. Photo of *the new refractory microstructure*

Overall, the microstructure for *the new* alumina *brick* sample showed a homogeneous structure, showed no cracks between grains and did not have large pores (Figure 7). The homogeneity of microstructure and chemical composition in the new alumina *refractory brick sample* is supported by mapping data as shown in Figure 8. The elements Al, Si, O are evenly distributed on the surface, along with the supporting chemical elements in the form of Ca, K and Ti are scattered in the matrix. While the element iron (Fe) is scattered in the matrix, but there are also groups at the grain boundary, but the chemical composition is relatively low overall.

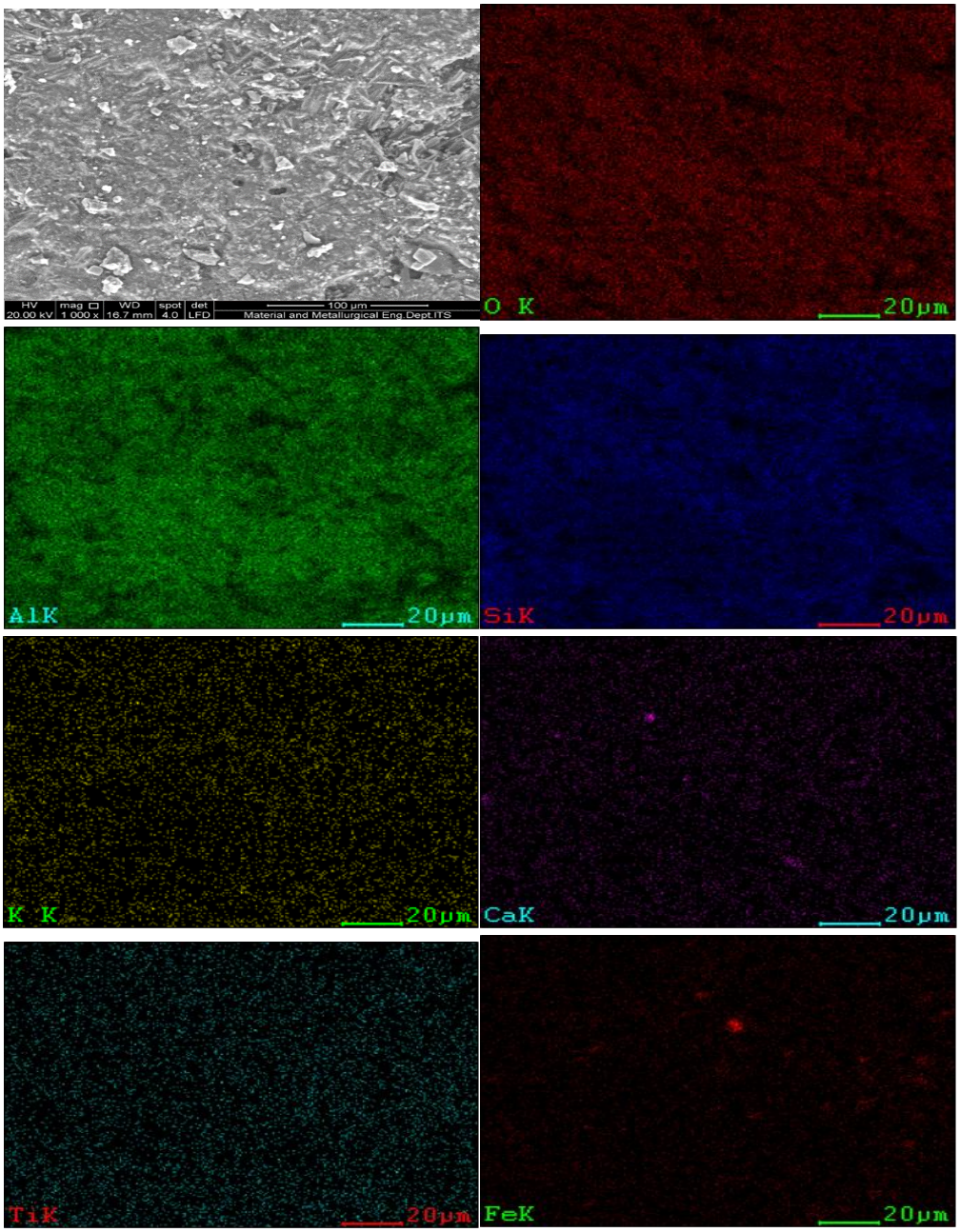

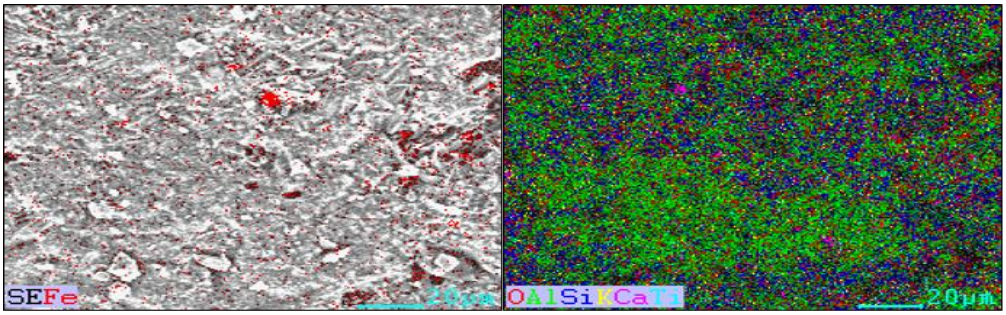

Figure 6. Results of mapping chemical composition in *a new refractory brick sample*

Table 3. EDX composition in a *new refractory brick sample*

Element	**Wt% (a)**	**Wt% (b)**	**Wt% (c)**
O K	35.27	32.60	34.96
By K	-	0.61	-
Mg K	-	0.76	-
Al K	38.27	30.26	35.62
Si K	26.46	27.85	25.80
K K	-	1.56	-
Ca K	-	1.63	-
From K	-	1.77	-
Fe K	-	2.96	3.63

The results of the SEM-EDX analysis show that this new refractory material has a composition consistent with alumina-silicate-based materials. The predominance of aluminum, oxygen, and silicon elements across the analysis points suggests that the main phase of this material is a combination of corundum (Al_2O_3), mullite ($3Al_2O_3 \cdot 2SiO_2$), and possibly *glassy phase*. The difference in the content of Fe and other minor elements between the analysis points summarized in Table 3 indicates the existence of a microstructural heterogeneity that is common in refractory materials.

This variation in composition also indicates that during the sintering process, local phase segregation occurs which causes the distribution of minor elements to be uneven. The presence of minor phases such as $FeAl_2O_4$ or other complex oxides can affect the refractory resistance to corrosion as well as thermal loads, which should be considered in the analysis of refractory performance during furnace operation.

The analysis of microstructure and chemical composition through SEM-EDX succeeded in identifying the presence of a multiphase structure in the new refractory, with the dominance of the alumina-silicate phase and the presence of minor phases. The presence of elements Fe, Ca, and Mg at the grain boundaries of the material can be a potential weak point that accelerates the rate of corrosion and slag penetration when the material is used in the furnace. Therefore, although in general the microstructure of this new refractory appears to be good, the results of the analysis indicate the need to be aware of potential degradation in areas with higher concentrations of minor elements.

Characterization of Used Refractory

This chapter discusses the characteristics of used refractories that have been exposed to operation in an Electric Arc Furnace (EAF). This analysis aims to evaluate the physical and

chemical changes that occur in the refractory material after undergoing thermal cycles and interactions with process materials during the operating period. Characterization of used refractory is carried out using methods similar to new refractory, namely through visual observation, chemical composition analysis with X-Ray Fluorescence (XRF), crystalline phase identification using X-Ray Diffraction (XRD), and observation of microstructure and elemental distribution using Scanning Electron Microscope-Energy Dispersive X-Ray (SEM-EDX). However, in used refractories, the test focus is more on changes in structure, composition, and phases due to the effects of slag corrosion and repeated heating-cooling cycles.

Visual Observation and Damage Zones

Visual observations of the used refractory refractories show significant structural degradation, especially on the side of the refractory that is directly exposed to the process environment. The change in color from pale beige to dark gray to brownish-black indicates oxidation, metal diffusion, and contamination of the process material. Three main zones can be clearly identified:

1. The Intak Refractory Zone, a part of the refractory that remains solid and homogeneous, resembles the initial condition without significant visual damage.
2. The Transition Zone, undergoes a discoloration and begins to show micro-cracks, texture changes, and softening due to partial chemical reactions.
3. Slag Zone, a refractory surface that is in direct contact with *slag*; appears partially melted, cracks widespread, and highly porous. This surface also experiences the accumulation of metal residues and scale.

Chemical Composition Change (XRF)

According to visual observation, the sample used refractory showed three areas with different chemical compositions. The results of XRF analysis on the used refractory showed a significant change in chemical composition compared to the new refractory. The content of alumina (Al_2O_3) was observed to decrease to below 20%, while the content of Fe_2O_3 increased sharply, reaching more than 60%.

Table 4. Comparison of XRF Test Results on Sample Used Refractory

Chemical Composition	% Wt				Information
	New Refractory brick	Refractory Area (D)	Transition Zone (E)	Stroke (F)	
Al2O3	39,49 - 44,77	40,58	22,74	15,71	Less and less
SiO2	34,00 – 36,00	36	22	14	Less and less
P2O5	5,80 - 7,20	5,8	2	0,6	Less and less
K2O	1,10 – 1,20	1,1	0,57	0,31	Less and less
CaO	1,30 – 1,40	1,4	0,91	0,85	Less and less
TiO2	2,03 – 2,21	2,21	0,72	-	Less and less
Fe2O3	11,00 – 12,5	12,5	48,1	62,52	Increasing
Cr2O3	-	0,15	0,36	1,46	Increasing
Nürnü	-	0,2	2,59	4,87	Increasing

Table 4. presents a comparison of the oxide element content in new refractory bricks and used bricks that have been exposed to the furnace operating environment, covering three main zones: Refractory Area (D), Transition Zone (E), and Slag Penetration (F) area. The analysis was carried out using the X-Ray Fluorescence (XRF) method to identify changes in chemical composition due to thermal corrosion and chemical interactions with slag.

The main component in refractory bricks, Al_2O_3, shows a significant decrease in concentration from the initial value of 39.49–44.77 wt% in new bricks to 15.71 wt% in the slag zone. This phenomenon reflects the decomposition and lubrication of alumina due to reactions with the active components in slag, especially Fe_2O_3 and SiO_2. A similar decrease was also observed in the SiO_2 content which decreased from the range of 34–36 wt% in the new brick to only 14 wt% in the F zone, indicating the dissolution of silica into slag due to high temperatures and ionic diffusion processes during operation.

Other minor elements such as P_2O_5, K_2O, CaO, and TiO_2 also show a gradual downward trend from the refractory area to the slag zone. The P_2O_5 content decreased drastically from 5.8 wt% to 0.6 wt%, while K_2O and CaO decreased to 0.31 wt% and 0.85 wt%, respectively. This indicates that these elements tend to dissolve easily and detach from the crystalline structure of bricks when exposed to high temperatures and corrosive media. TiO_2 which was initially 2.03–2.21 wt% also decreased to be undetectable in the F zone, indicating that titanium was decomposed or carried into the slag liquid phase.

In contrast to the previous element, Fe_2O_3 experienced a drastic increase from the initial value of 11.00–12.5 wt% in the new brick to 62.52 wt% in the slag zone. These spikes indicate the penetration and diffusion of Fe from slag into the pores and refractory microstructures, as well as the possible formation of a spinel hercynite ($FeAl_2O_4$) phase that triggers brick degradation through volumetric expansion and thermal cracking. The increase in Fe_2O_3 levels in the transition zone by 48.1 wt% also strengthens the hypothesis that iron oxide is a major factor in the refractory corrosion process.

In addition, undetected elements of Cr_2O_3 and NiO in new bricks began to appear in the used zone with a gradually increasing concentration, reaching 1.46 wt% (Cr_2O_3) and 4.87 wt% (NiO) in the slag zone. The presence of these two oxides indicates contamination of the melting process raw material (calcine) that melts at high temperatures, which is carried into the refractory system through splashing or diffusion. This is also an indicator that corrosion is not only thermal, but also metallurgical, because it involves metals transitioning from the smelting process.

Overall, the pattern of element distribution in the table shows progressive degradation of alumina refractory bricks due to a combination of chemical corrosion by slag, metal contamination, and the release of the original elements from the refractory material. The chemical transitions recorded in the E zone show an important role as a region between surviving and severely damaged materials, so they can be used as an early indicator of refractory damage in the evaluation of furnace life.

Crystalline Phase Transformation (XRD)

To strengthen the results of the chemical composition analysis, crystalline phase identification was carried out through XRD. This analysis aims to uncover changes in

crystalline structure that occur due to the interaction between the refractory and slag as well as exposure to the thermal cycle during furnace operation.

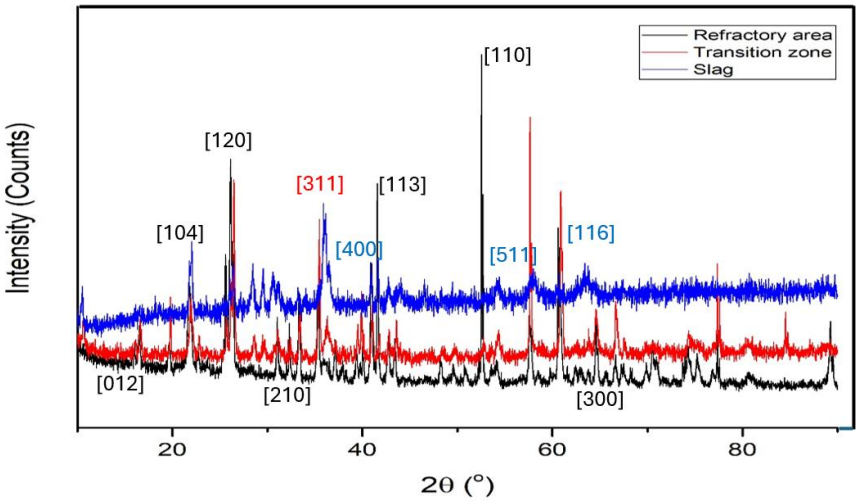

Figure 7. XRD Test Results on Sample Used Refractory in Refractory area (Black), transition zone (red) and Slag zone (blue)

Table 5. Results of Phase Identification and Quantitative Analysis on Sample Used Refractory Brick

Crystalline Phase	**% Wt**		
	***Refractory* Area**	**Transition Zone**	***Battle* Area**
Mullite ($3Al_2O_3 \cdot 2SiO_2$)	64.3	18.3	21.5
Corundum (α-Al_2O_3)	20.4	13.0	–
Cristobalite (SiO_2)	6.1	2.6	8.7
Andalusian (Al_2SiO_5)	8.2	–	–
Moganite (SiO_2)	–	16.5	–
Sillimanite (Al_2SiO_5)	–	27.8	5.6
Potassium Aluminum Silicate($KAlSi_2O_6$)	–	8.7	–
Mg-spinel ($mgAl_2O_4$)	0.5	6.9	9.5
Fe-Spinel ($FeAl_2O_4$)	0.5	6.1	11.8
Calcium Aluminum Oxide($Ca_5Al_6O_{14}$)	–	–	23.9
Magnesium Aluminum Silicate Hydrate($Mg_2Al_4Si_5O_{18} \cdot 0.54H_2O$)	–	–	19.1

The results of the x-ray diffraction test on the refractory used sample are shown in Figure 7 The diffraction pattern shows that there are several differences in diffraction peaks in each test sample, these differences lead to differences in compounds/phases identified as part of the qualitative analysis. Qualitative and quantitative analysis using High-score plus analysis software is shown in Table 5.

Based on XRD analysis in the refractory area, alumina bricks still show a very intact and homogeneous crystalline structure. Mullite—the result of sintering between Al_2O_3 and SiO_2—accounted for about 64% of the overall phase, while corundum stuck strongly at 20%. The presence of minor sillimanite (~8 %) and cristobalite (~6 %) only marks the remainder of the

thermal reaction of brick-making, without disturbing the cohesion of the matrix. Spinel $MgAl_2O_4$ and $FeAl_2O_4$ are almost undetectable (< 1%), proving that prior to slag contact, the reaction of Al_2O_3 with metal oxides is virtually non-existent. These conditions explain why these zones maintain optimal thermal and mechanical rigidity in operating temperatures.

The results of XRD in the transition area also showed a radical change. The mullite content shrinks drastically to 18%, while corundum drops to 13%, signaling partial dissolution by the molten phase of slag. The decomposition of mullite gives rise to sillimanite (27.8%) and moganite (16.5%), recrystalline silica phases that indicate thermal and chemical imbalances. At the same time, spinels begin to form: $MgAl_2O_4$ reaches ~7 % and $FeAl_2O_4$ ~6 %, totaling about 14 %. The presence of potassium aluminum silicate (≈ 8.7 %) indicates alkaline infiltration of slag, while cristobalite drops to 2.6 % due to the dominance of new corrosive phase formation. This zoning marks the region where bricks begin to lose grain integrity and the bonds between crystals weaken.

In the slag area, the primary structure is almost completely eroded. Mullite remains 21.5%, while corundum practically vanishes. Spinel grew rapidly to 21.3% (divided by 9.5% Mg-spinel and 11.8% Fe-spinel), while the corrosive silicate phase took over: calcium aluminum oxide ($Ca_5Al_6O_{14}$) by 23.9% and magnesium aluminum silicate hydrate ($Mg_2Al_4Si_5O_{18}\cdot 0.54H_2O$) by 19.1%. Cristobalite also rose again to 8.7%, marking the transformation of silica to an amorphous/glassy form. The combination of expansive spinel and brittle silicates creates a matrix that is low cohesion and prone to cracking.

Overall, the evolution of the composition from the refractory area to the slag area maps the path of degradation: the initiation of spinelization reactions at the grain border, followed by the corundum/mullite dissolution by the molten phase of the slag, and finally the accumulation of the brittle phase on the most exposed surface. This transformation is driven by high temperatures (> 1 184 °C) and diffusion of Fe^{2+}/Mg^{2+} ions, resulting in volumetric expansion that triggers microcracks. The daily heating-cooling cycle then doubles the crack into macroscopic spalling. These results confirm that design interventions—whether anti-spinel-coated brick formulations or roof geometry adaptations—are indispensable to reduce the rate of degradation and extend the service life of EAF refractories.

To complete the crystallographic analysis, microstructure observations using SEM-EDX were carried out to identify changes in texture and distribution of elements in more detail. This analysis is important to understand the mechanism of degradation at the microscale that occurs during furnace operation.

Microstructure and Element Mapping (SEM/EDX)

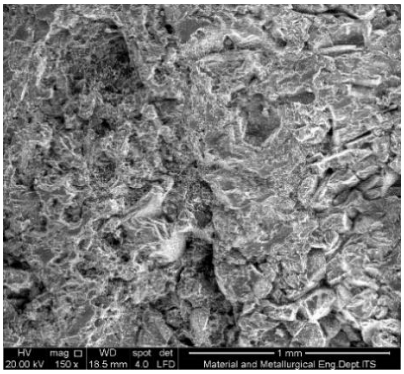

(a)

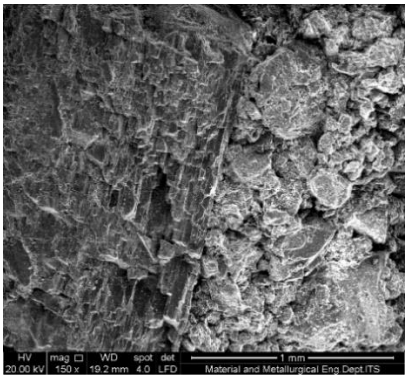

(b)

(c)

Figure 8. Comparison of Microstructures in Used Refractory Brick

(a) Refractory Area, (b) Transition Zone and (c) Slag Area

SEM/EDX testing is performed on samples used refractory for further analysis to determine changes in the microstructure and distribution of chemical composition. Figure 8 is a summary of the comparison of microstructures in three areas used refractory. Figure 8 (a) shows the microstructure for the refractory area, the grain size becomes smaller but still shows the homogeneity of the microstructure. Figure 8 (b) shows the transition area, where there is a difference in the refractory and slag boundary areas. The left side correlates with the refractory microstructure while the right side corresponds to the refractory area slag. The microstructure in the slag area of Figure 8(c) shows a heterogeneous particle size. Specifically, in each area used refractory, EDX composition analysis and specific observations were carried out as shown in Table 6.

Table 6. EDX-based composition in various zones used refractory brick

Element	**Wt%**				
	(Refractory Area)	**Transition Zone)**	**(Battle Area)**	**(Battle Area)**	**(Battle Area)**
O K	39.59	31.51	23.64	21.22	24.03
By K	-	0.54	0.99	-	-

Element	Wt%				
	(Refractory Area)	Transition Zone)	(Battle Area)	(Battle Area)	(Battle Area)
Mg K	-	2.24	3.65	3.37	2.97
Al K	39.10	23.08	12.51	8.47	10.81
Si K	18.53	13.98	9.13	3.46	2.17
Ca K	-	0.65	-	-	-
Fe K	2.78	28.01	50.08	61.52	60.02
By K	-	-	-	1.97	-

Based on EDX data, it can be explained that used refractory bricks have a different chemical composition. In the refractory area, the composition still shows the suitability of the composition with the new refractory, this shows that even in the used sample, degradation does not occur simultaneously. A review of the transition area shows that the chemical composition changes as the position changes.

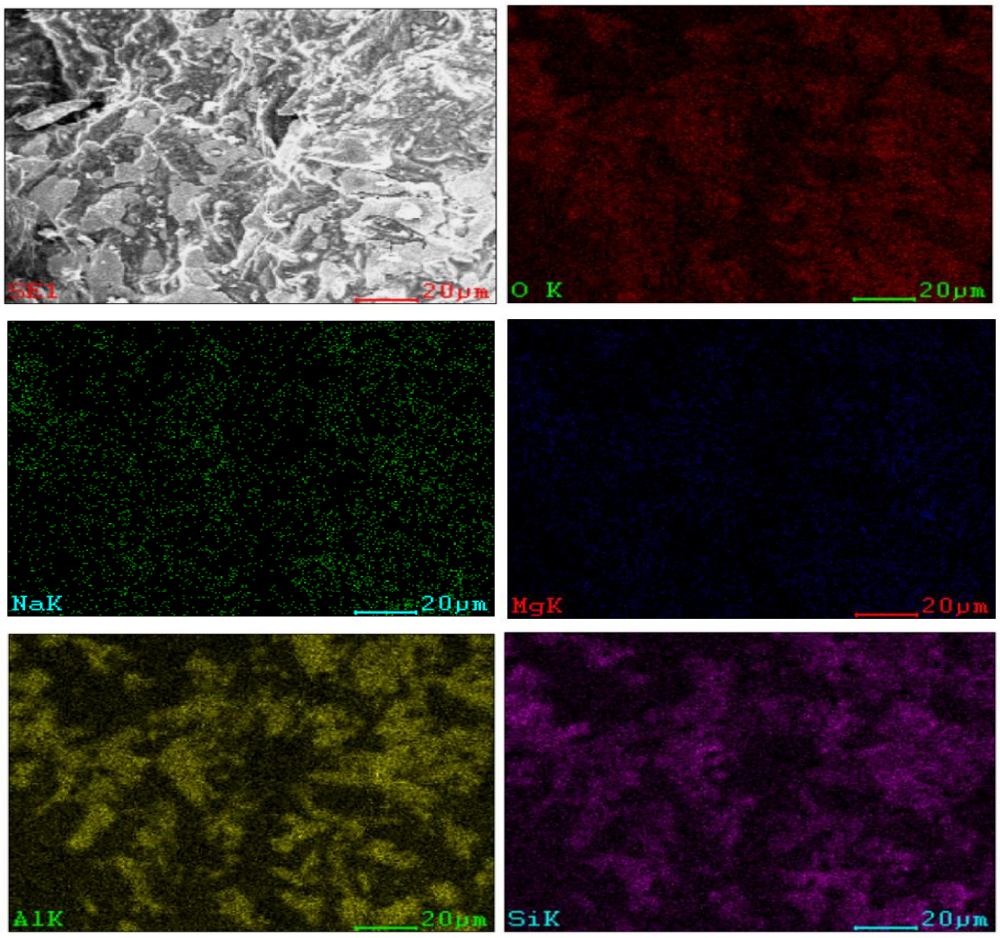

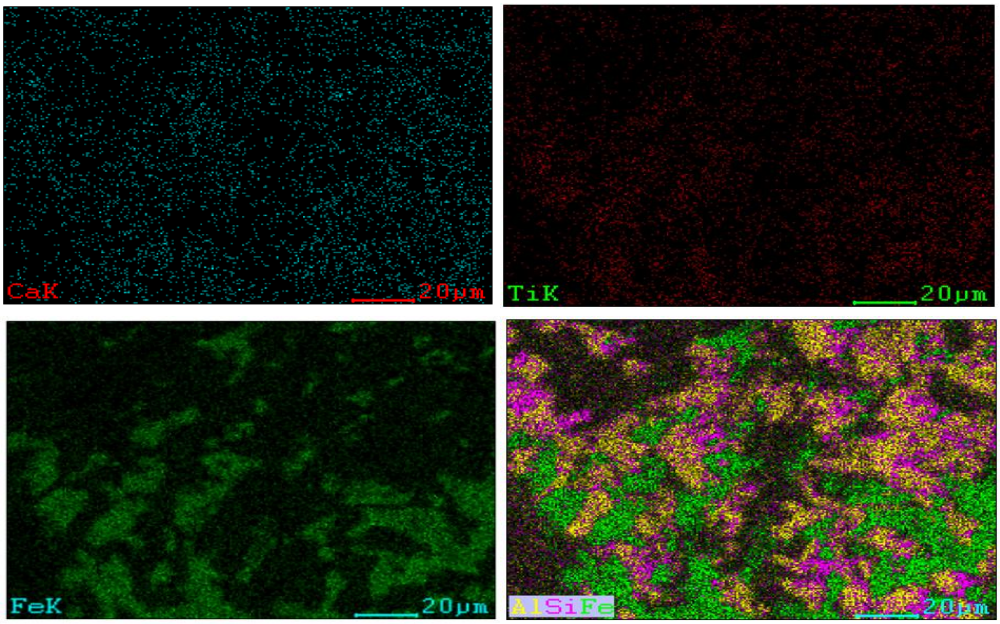

Figure 10. Results of SEM/EDX Elemental Mapping in Refractory Slag Areas

CONCLUSION

This research identified key degradation mechanisms in 70% alumina refractory bricks used in electric arc furnace roofs through an integrated approach combining material analysis, thermodynamic modeling, and thermal stress simulations. New bricks primarily contained corundum and mullite phases, while used samples showed harmful formation of hercynite and spinel due to high-temperature slag reactions, increasing porosity and weakening the material. Thermal stress analysis highlighted the unsupported central filler area as a critical failure zone where stresses exceeded tensile limits, indicating the need to urgently redesign the F-type brick hanger and tertiary beam system to reduce stress concentrations. The study establishes a multidisciplinary framework for understanding refractory failure and provides practical recommendations, including implementing advanced thermo-mechanical simulations for structural improvement and deploying AI-driven real-time sensor monitoring for early failure detection and maintenance optimization. Future research should focus on techno-economic assessments of these designs via multi-scenario simulations and the creation of a field-data-driven refractory degradation database to enhance predictive capabilities and operational decision-making.

REFERENCES

Abdelmoula, M., Küçüktürk, G., Juste, E., & Petit, F. (2024). Enhancing powder bed fusion of alumina ceramic material: A comprehensive study from powder tailoring to mechanical performance evaluation. *The International Journal of Advanced Manufacturing Technology*.

Chen, Y., Liu, H., & Zhang, L. (2020). Thermal and chemical resistance of alumina-based refractories under high-temperature industrial conditions. *Ceramics International, 46*(12), 20021–20030. https://doi.org/10.1016/j.ceramint.2020.04.123

Dalvi, A. D., Bacon, W. G., & Osborne, R. C. (2020). The past and the future of nickel laterites.

Minerals Engineering, 146, 106142. https://doi.org/10.1016/j.mineng.2019.106142

Darban, S., Cassayre, L., Chiartano, S., Lacarrière, L., Cyr, M., Patapy, C., & Prigent, P. (2023). Corrosion mechanisms of Al_2O_3–SiC–C refractory castables by iron and slag based on post-mortem analysis of industrial samples. *Open Ceramics, 16*, 100453.

Gupta, S., & Kumar, A. (2020). Nickel smelting technologies and advances in electric arc furnace applications. *Minerals Engineering, 155*, 106482. https://doi.org/10.1016/j.mineng.2020.106482

Hernández, J., Morales, F., & Torres, R. (2020). Refractory degradation mechanisms in pyrometallurgical furnaces. *Journal of Materials Processing Technology, 285*, 116814. https://doi.org/10.1016/j.jmatprotec.2020.116814

Kuang, Z., Yin, M., Jia, Z., Li, X., & Yu, S. (2025). The preparation of highly transparent alumina ceramics with excellent mechanical performance via co-doping strategy. *Journal of Alloys and Compounds*.

Li, W., & Wang, J. (2021). Performance evaluation of alumina-based refractories for high-temperature furnace applications. *Journal of the European Ceramic Society, 41*(1), 455–466. https://doi.org/10.1016/j.jeurceramsoc.2020.08.015

Li, W., Zhang, M., & Wang, J. (2021). Performance evaluation of alumina refractory linings in high-temperature metallurgical furnaces. *Journal of the European Ceramic Society, 41*(6), 3451–3463. https://doi.org/10.1016/j.jeurceramsoc.2021.01.034

Rodrigues, M., Pereira, L., & Costa, A. (2022). Failure analysis and lifespan prediction of industrial refractory linings. *Engineering Failure Analysis, 138*, 106330. https://doi.org/10.1016/j.engfailanal.2022.106330

Silva, R., & Gomes, A. (2021). Slag–refractory interactions in metallurgical processes: Mechanisms and mitigation. *Metallurgical and Materials Transactions B, 52*(4), 1988–2002. https://doi.org/10.1007/s11663-021-02099-w

Sun, Y., Li, S., Zhao, Q., Cong, Z., Xia, Y., Jiao, X. H., & Chen, D. (2025). Recent advancements in alumina-based high-temperature insulating materials: Properties, applications, and future perspectives. *High-Temperature Materials*.

Wang, Z., Jiang, Y., Baiker, A., & Huang, J. (2020). Pentacoordinated aluminum species: New frontier for tailoring acidity-enhanced silica–alumina catalysts. *Accounts of Chemical Research*.

Zhang, L., & Ostrovski, O. (2018). High-temperature smelting of nickel laterites in electric furnaces: Thermodynamics and operational challenges. *Journal of Cleaner Production, 175*, 523–533. https://doi.org/10.1016/j.jclepro.2017.12.067

Zhao, X., Liu, Y., & Zhang, P. (2019). Temperature distribution and thermal stress analysis in electric arc furnaces. *Journal of Cleaner Production, 231*, 1082–1091. https://doi.org/10.1016/j.jclepro.2019.05.325

Zheng, J., Pang, Q., Hu, Z., & Sun, Q. (2022). Recent progress on regulating strategies for the strengthening and toughening of high-strength aluminum alloys. *Materials*.